JOURNAL OF MATERIALS SCIENCE 27 (1992) 3335–3340

Sintering of $Li_xNi_{1-x}O$ solid solutions at 1200 °C

E. ANTOLINI
Ansaldo Ricerche, Corso Perrone 25, 16152 Genova, Italy

The sintering process of $Li_xNi_{1-x}O$ solid solutions, with different x values, was examined. Sintering was performed in air at 1200 °C. An intense shrinkage in lithiated nickel oxide, with respect to the undoped NiO, was observed. This behaviour is attributed to the existence of a gradient in the chemical potential of the lithium ion between the surface and the interior of the particles, due to lithium oxide evaporation, which acts as the driving force of the mass transport by volume diffusion.

1. Introduction

The molten carbonate fuel cell (MCFC) is an efficient device for electrochemical conversion of chemical energy to electrical energy [1, 2]. The state-of-the-art MCFC consists of a porous nickel (containing dispersed chromium to provide strength and sintering resistance) anode (fuel electrode), a porous lithium-doped nickel oxide cathode (oxidant electrode), and a lithium aluminate matrix filled with lithium and potassium carbonates (62–70 mol % Li_2CO_3) as the electrolyte.

NiO is a p-type semiconductor [3, 4]; thus, when it is used as the cathode material in the fuel cell, its conductivity is enhanced by doping with lithium. The incorporation of lithium into NiO results in the formation of an Ni^{3+} content equivalent to the amount of lithium added to the solution (Ni^{2+} is replaced by Ni^{3+}) [3, 4].

X-ray studies indicate a homogeneous crystal of the same structure as the initial nickel oxide but with a somewhat smaller unit cell. The reaction resulting in this product can be represented as

$$x/2\,Li_2O + (1 - x)\,NiO + x/4\,O_2 \rightarrow Li_x^+ Ni_{1-2x}^{2+} Ni_x^{3+} O \quad (1)$$

Consequently, the electronic conductivity of NiO increases significantly, due to the exchange of electron holes between nickel ions of 2 + and 3 + valence states.

The preparation method of $Li_xNi_{1-x}O$ structures starts from Li_2CO_3 and nickel powders [5]. The green powder and binder are heated in air for conversion to $Li_xNi_{1-x}O$; temperatures sufficient to sinter $Li_xNi_{1-x}O$ lead to large Li_2O volatilization losses (as is known [6], Li_2O evaporation essentially occurs at temperatures higher than 1000 °C), while lower temperature treatments yield a product of inferior strength or improper morphology.

Previous work [7] has demonstrated that the amount of lithium carbonate in the starting mixture affects the sintering behaviour of mixed lithium–nickel oxide cathodes. The aim of the present work was to evaluate whether the sintering of the compact was related to Li_2O evaporation (contribution of this flux of the mass to the total flux of the material by the mechanism of volume diffusion) or to the Li^+ presence in the solid solution (increase of the diffusion coefficient of the nickel ion in NiO, due to the possible presence of lattice defects, such as vacancies, owing to the addition of lithium ions; it is known [8], that $Li_xNi_{1-x}O$ solid solutions of high lithium content contain appreciable concentrations of lattice defects). For this purpose, nickel and lithium carbonate powders were mixed in the proper ratio to yield $Li_xNi_{1-x}O$ with $x = 0.00$, 0.06 and 0.12 after firing. The behaviour of these solid solutions was followed through isothermal heat treatment at 1200 °C, a temperature at which both sintering and evaporation processes are easily detectable.

2. Experimental procedure

2.1. Sample preparation

Nickel Inco 255 and lithium carbonate Merck 5671 were used as starting materials. Mixtures of these powders (in the compositions 0.00, 0.06, and 0.12 mol % Li^+) were ball milled for 24 h in a polyethylene container together with a binder (Methocel MC Fluka Chemie 64620, 400 mPa), an antifoam agent (Dow Corning antifoam A compound) and deionized water. The samples with different density, but equal composition, were obtained by varying the nickel/binder ratio in the slurry. The resulting slurries were degassed and then cast on to bee's wax-coated glass surfaces; after the tapes were dried, disc-shaped samples (diameter 5 cm) were finally cut from them with a razor blade and a template. The thickness of the samples obtained was 0.50 mm. The sample plaques were then put on porous alumina platforms and subjected to the following thermal cycle:

(a) heating at 1.0 °C min^{-1} from room temperature to 1200 °C;

(b) isothermal holding at 1200 °C for times in the range 0–20 h;

(c) cooling at 1.0 °C min^{-1} from 1200 °C to room temperature.

Thermal treatments were performed in air using a

0022–2461

BICASA BE 35 furnace. The plaque diameter was measured before and after thermal treatment by a digital caliper (Facom No1742.1). The overall precision of the measurements was $\pm 10^{-2}$ mm.

2.2. X-ray diffraction (XRD) measurements

Diffraction data were obtained by a Philips PW1710 powder diffractometer equipped with a Philips PW1050 vertical goniometer using CuK_α radiation, monochromatized by a graphite bent-crystal monochromator. Spectra have been collected up to reflection (5 1 1) of nickel oxide at a scanning rate of $0.05° s^{-1}$. Diffraction maxima were obtained in step-scan mode (step 0.02°, counting time 1 s). Lattice constant values were obtained by a least squares refinement based on a cubic lattice.

2.3. Density

Density values were determined using Archimedes' method in mercury. The theoretical density, δ_{th}, of the solid solutions was determined from the lattice constants and the lithium content at the beginning of the isothermal soak, from the following relationship (all samples crystallized in the cubic rocksalt structure):

$$\delta_{th} = 4[xM_{Li} + (1 - x)M_{Ni} + M_O]/l^3 N_A \quad (2)$$

where M_{Li}, M_{Ni} and M_O are the atomic masses of lithium, nickel and oxygen, respectively, x is the lithium atomic fraction in the solid solution at $t = 0$; l(cm) is the lattice constant and N_A is Avogadro's number. x is calculated from the lattice constant from the relation [7]

$$x = \frac{0.41748 - l(\text{nm})}{0.017756} \quad (3)$$

2.4. Scanning electron microscopy (SEM)

Scanning electron micrographs were collected by a Cambridge Stereoscan 200 scanning electron microscope. Scale bars, accelerating voltage (kV) and working distance (WD) are reported on each micrograph. Pure nickel oxide samples were gold sputtered (gold thickness about 15 nm). No sputtering was necessary on lithium-containing samples.

3. Results

3.1. Plaque diameter change

The dependence of plaque diameter change following thermal treatment, $\Delta L/L_g$ (where L_g is the initial diameter of the compact powder and ΔL is the diameter change) on isothermal time at 1200 °C for $Li_xNi_{1-x}O$ is shown in Fig. 1. The data show an increase in the shrinkage of the samples with time for all the compositions. The difference in the $\Delta L/L_g$ values at $t = 0$ h depends on the effect of the different lithium contents during the heating step (plaque dilatation up to 900 °C, followed by plaque shrinkage from 900–1200 °C) [7].

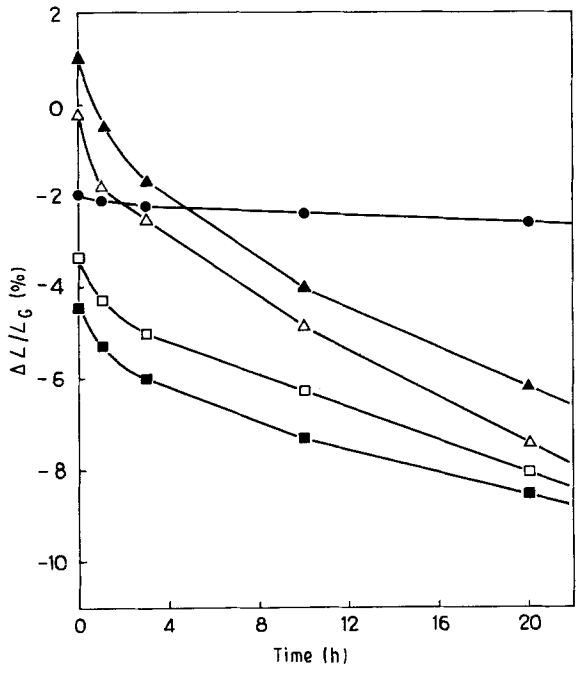

Figure 1 Time dependence of plaque diameter change following thermal treatment, $\Delta L/L_g$ at 1200 °C for $Li_xNi_{1-x}O$ at various x values and densities: (●) $x = 0.00$, (□) $x = 0.06$ L, (■) $x = 0.06$ H, (△) $x = 0.12$ L, (▲) $x = 0.12$ H. L = lower density sample, H = higher density sample.

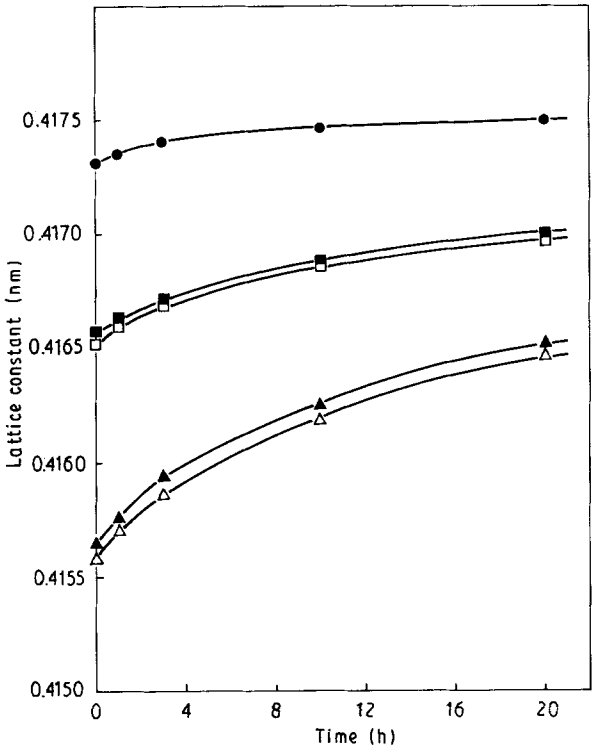

Figure 2 Dependence of the lattice constant on isothermal time at 1200 °C for $Li_xNi_{1-x}O$ at various x values and densities: (●) $x = 0.00$, (□) $x = 0.06$ L, (■) $x = 0.06$ H, (△) $x = 0.12$ L, (▲) $x = 0.12$ H. L = lower density sample, H = higher density sample.

3.2. XRD measurements

Fig. 2 shows the dependence of lattice constant of pure and lithium-doped samples on isothermal times. The lattice constant increases with increasing time: a rela-

TABLE I Material densities and porosity

Nominal Li^+ (mol %)	Green density ($g\ cm^{-3}$)	Experimental density ($t = 0$), δ_s ($g\ cm^{-3}$)	Theoretical density, δ_{th} ($g\ cm^{-3}$)	Porosity $1 - \delta_s/\delta_{th}$ ($t = 0$) (%)
0	2.19	2.69	6.82	61
6	1.51	1.92	6.62	71
6	2.20	2.74	6.61	59
12	1.94	2.02	6.42	68
12	2.25	2.43	6.40	62

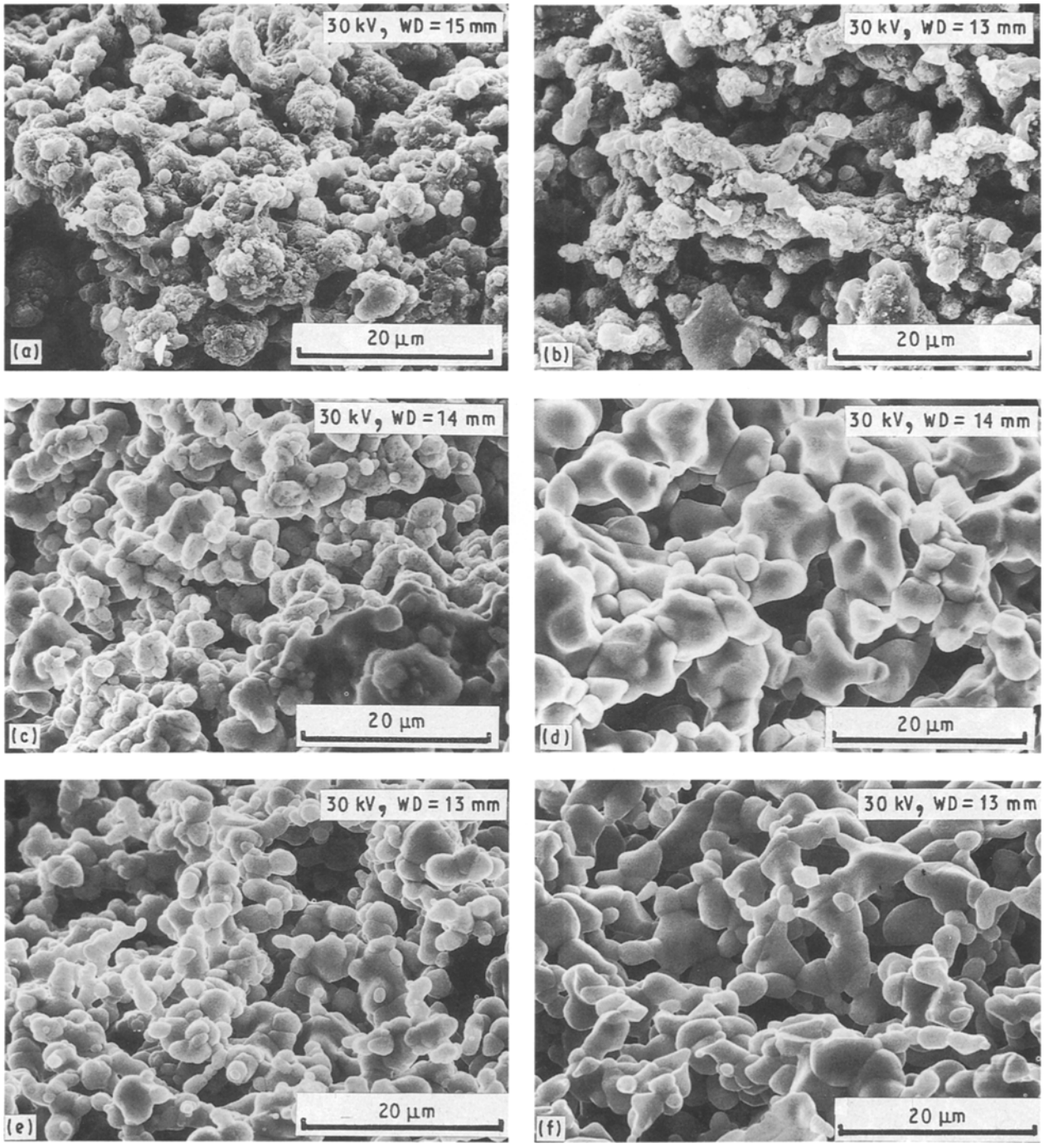

Figure 3 Scanning electron micrographs of $Li_xNi_{1-x}O$ plaques following thermal treatment at 1200 °C for (a) $x = 0.00$, 0 h; (b) $x = 0.00$, 20 h; (c) $x = 0.06$, 0 h; (d) $x = 0.06$, 20 h; (e) $x = 0.12$, 0 h; (f) $x = 0.12$, 20 h.

tionship exists between lattice constant and lithium content in $Li_xNi_{1-x}O$ solid solution [7]

$$l\,(\text{nm}) = 0.41748 - 0.01756\,x \qquad (3')$$

where l (nm) is the lattice constant and x is the lithium atomic fraction in the solid solution. This means that during thermal treatment, lithium loss from the solid solution occurs.

3.3. Density

Table I shows the green density, density at beginning of the isothermal step, theoretical density and total porosity, calculated from density measurements.

Green density depends on the compositions of the starting mixture; density at $t = 0$ depends on green density and on lithium carbonate content in the starting mixture [7]; theoretical density decreases with increasing lithium content in the solid solution.

3.4. SEM

The sintered network of $Li_xNi_{1-x}O$ solid solutions developed by heating at 1200 °C for 0 and 20 h is shown in Fig. 3a–e. The micrographs of undoped NiO (Fig. 3a and b show no appreciable differences. For the 6 and 12 mol % Li^+ samples the following changes in the microstructure were observed: (1) smaller particles (or grains) disappear, while larger particles become larger, i.e. coarsening has occurred; (2) groups of grains are rearranged relative to others; (3) new interparticle contacts are made.

4. Discussion

Solid-state sintering involves material transport by diffusion. Diffusion can consist of movement of atoms or vacancies along a surface or grain boundary or through the volume of the material. Surface diffusion, like vapour-phase transport, does not result in shrinkage. Volume diffusion, whether along grain boundaries or through lattice dislocations, does result in shrinkage [9]. A shrinkage law of the type

$$\Delta L/L_o = kt^n \tag{4}$$

is commonly observed during the initial stages of sintering, where L_o is the initial length of the compact, ΔL is the change in that dimension and t is time. The value of exponent n is related to the particular mechanism for material transport. From the $\Delta L/L_g$ values for isotherm times, t, $t = 0$, we obtain

$$\Delta L/L_o(t) = \frac{\Delta L/L_g(t) - \Delta L/L_g(t=0)}{1 + \Delta L/L_g(t=0)} \tag{5}$$

Fig. 4 shows the log–log plot of shrinkage of (Li, Ni)O compacts versus time: the slope of these lines, i.e. the value of n, is around 0.5, which is representative of material transport by volume diffusion through lattice dislocations [10]. As shown in Table II, the sintering rate constant, k, increases with increasing nominal lithium content in the mixture; the effect of the different density (porosity) on k, the nominal Li^+ molar fraction being equal, is negligible.

As shown in Fig. 3, scanning electron micrographs attest the results of shrinkage measurements: pure NiO shows no appreciable change in the microstructure, while lithium-containing samples show a transformation in the network and size of the particles going from isotherm time $t = 0$ to $t = 20$ h.

As shown in Section 3.2, for a solid solution with no appreciable concentration of lattice defects different from substitutional ones, from the values of the lattice constant, through Equation 4, the Li^+ cationic fraction after thermal treatment may be calculated. From initial ($t = 0$ h) and final lithium contents in the solid solution, the evaporated Li^+ molar fraction has been calculated. We start from

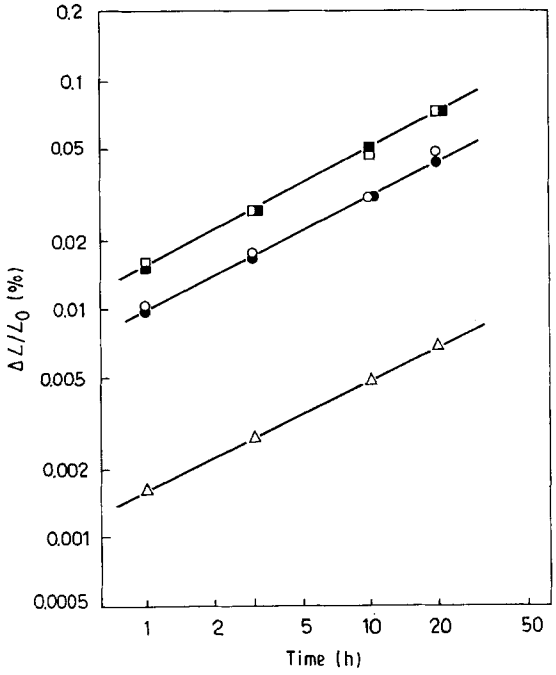

Figure 4 Log–log plots of shrinkage at 1200 °C for $Li_xNi_{1-x}O$ at various x values and densities: (△) $x = 0.00$, (○) $x = 0.06$ L, (●) $x = 0.06$ H, (□) $x = 0.12$ L, (■) $x = 0.12$ H. L = lower density sample, H = higher density sample.

TABLE II Sintering rate constant, k, and exponent, n, values for pure and lithium-doped NiO

Nom. mol % Li^+ [a]	n	$k(h^{-n})$
0	0.48	0.002
6 H	0.50	0.010
6 L	0.50	0.010
12 H	0.53	0.015
12 L	0.49	0.016

[a] L = lower density sample, H = higher density sample.

$$x_{ev} = \frac{\text{mol Li}_{ev}}{\text{mol Li}(t=0) + \text{mol NiO}} = \frac{\text{mol Li}(t=0) - \text{mol Li}(t)}{\text{mol Li}(t=0) + \text{mol NiO}} \tag{6}$$

It follows that:

$$x_{ev} = x(t=0) - \left[\frac{\text{mol Li}(t)}{\text{mol Li}(t=0) + \text{mol NiO}}\right] \times \left[\frac{\text{mol Li}(t) + \text{mol NiO}}{\text{mol Li}(t) + \text{mol NiO}}\right] \tag{7}$$

$$x_{ev} = x(t=0) - x(t) \times \frac{\text{mol Li}(t=0) - \text{mol Li}_{ev} + \text{mol NiO}}{\text{mol Li}(t=0) + \text{mol NiO}} \tag{8}$$

$$x_{ev} = x(t=0) - x(t)(1 - x_{ev}) \tag{9}$$

Finally

$$x_{ev} = \frac{x(t = 0) - x(t)}{1 - x(t)} \quad (10)$$

Table III shows the values of Li^+ molar fraction in a solid solution $x(t)$ and evaporated $x_{ev}(t)$ following thermal treatment: obviously, the amount of evaporated Li^+ increases with increasing lithium content in the solid solution. From the x value at isothermal time $t = 0$, it is inferred that part of lithium oxide is lost during the dynamic step.

In Fig. 5, where $\Delta L/L_0$ is plotted against evaporated Li^+ molar fraction, the data show an approximately linear dependence of shrinkage (sintering rate) on lithium oxide loss. This behaviour seems to support the hypothesis that the driving force for the sintering process is lithium oxide evaporation.

For undoped NiO, we have seen that with increasing isothermal holding time the lattice constant increases and plaque colour changes from dark green to bright green: this indicates that the concentration of vacancies (deviation from the stoichiometric composition) decreases.

The interaction of Ni^{3+} with the atmosphere, which results in a local change of the chemical composition, leads to the formation of an oxygen chemical potential gradient between the surface and interior of the particle [11]. The existence of a gradient in the chemical potential of oxygen is an additional driving force in the sintering process, i.e. of the mass transport by volume diffusion: we must take into account the contribution of this flux of the mass to the total flux of the material by the mechanism of volume diffusion. The oxygen separation (loss) occurs, according to the reaction

$$2Ni^{3+} + O^{2-} + V_{Ni} \rightarrow 2Ni^{2+} + 1/2\,O_2 \quad (11)$$

In the same way, Li_2O evaporation leads to the formation of a lithium chemical potential gradient between the surface and the interior of the particle. This Li^+ chemical potential gradient acts as the driving force of the mass transport by volume diffusion; lithium oxide loss occurs according to the reaction

$$2Ni^{3+} + 2Li^+ + 2O^{2-} \rightarrow 2Ni^{2+} + Li_2O + 1/2\,O_2 \quad (12)$$

In the present sintering process, the effect of density (porosity) seems to be negligible.

TABLE III Actual Li^+ atomic fraction (%) in the solid solution and evaporated Li^+ atomic fraction (%) from $Li_xNi_{1-x}O$ following the isothermal step

Nominal Li^+ (mol %)	Isotherm time (h)	Actual Li^+ (mol %)	Evaporated Li^+ (mol %)
6 L	0	5.1	0.0
	1	4.6	0.5
	3	4.2	0.9
	10	3.3	1.9
	20	2.5	2.7
6 H	0	5.4	0.0
	1	4.8	0.6
	3	4.3	1.1
	10	3.4	2.1
	20	2.7	2.8
12 L	0	10.7	0.0
	1	10.1	0.7
	3	9.2	1.7
	10	7.4	3.6
	20	5.7	5.3
12 H	0	10.3	0.0
	1	9.7	0.7
	3	8.7	1.8
	10	7.1	3.4
	20	5.4	5.2

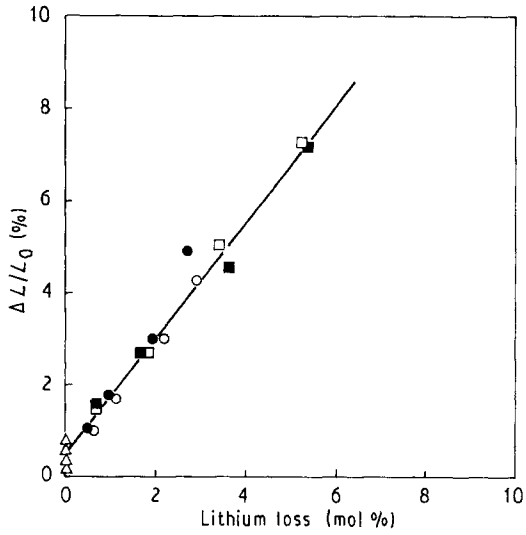

Figure 5 Dependence of shrinkage on lithium loss at 1200 °C for $Li_xNi_{1-x}O$ at various x values and densities: (△) $x = 0.00$, (●) $x = 0.06$ L, (○) $x = 0.06$ H, (■) $x = 0.12$ L, (□) $x = 0.12$ H. L = lower density sample, H = higher density sample.

5. Conclusion

The intense shrinkage in lithiated nickel oxide, with respect to the undoped NiO, is attributed to the existence of a gradient in the chemical potential of lithium which acts as the driving force of the mass transport by volume diffusion. Thus, the sintering process seems to be related to the amount of evaporated lithium oxide, rather than to the lithium content in the solid solution.

In the light of the behaviour of these solid solutions, it is possible to fabricate $Li_xNi_{1-x}O$ cathodes with predetermined lithium contents and degrees of sintering by pre-arranging the amount of Li_2CO_3 in the starting mixture.

References

1. J. R. SELMAN and L. G. MARIANOWSKI, in "Molten Salt Technology", edited by D. G. Lovering (Plenum, New York, 1982) pp. 323–93.
2. Morgantown Energy Technology Center, "Fuel Cells. A Handbook", DOE/METC-88/6096, May 1988.
3. D. ADLER, in "Solid State Physics", Vol. 21, edited by F. Seitz, D. Turnbull and H. Ehrenreich (Academic Press, New York, 1968) p. 1.
4. J. B. GOODENOUGH, in "Progress in Solid State Chemistry", Vol. 5, edited by H. Reiss (Pergamon Press, New York, 1971) p. 271.
5. C. E. BAUMGARTNER and K. P. ZARNOCH, *Amer. Ceram. Soc. Bull.* **64** (1985) 593.

6. Y. IIDA, *J. Amer. Ceram. Soc.* **43** (1960) 171.
7. E. ANTOLINI, M. LEONINI, V. MASSAROTTI, A. MARINI, V. BERBENNI and D. CAPSONI, *Solid State Ionics* **39** (1990) 251.
8. A. MARINI, V. BERBENNI, V. MASSAROTTI, G. FLOR, R. RICCARDI and M. LEONINI, *ibid.* **32/33** (1989) 398.
9. W. D. KINGERY, H. K. BOWEN and D. R. UHLMANN, "Introduction to Ceramics", 2nd Edn (Wiley, New York, 1976) pp. 469–90.
10. F. THUMMLER and W. THOMMA, *Metals Mater.* **1** (1967) 69.
11. S. B. BOSKOVIC and B. M. ZIVANOVIC, *J. Mater. Sci.* **9** (1974) 117.

Received 6 March
and accepted 1 July 1991